LAWRENCE
LIVERMORE
NATIONAL
LABORATORY

UCRL-JRNL-207910

Formation of Carbon Nanostructures in Cobalt- and Nickel-Doped Carbon Aerogels

R. Fu, T. F. Baumann, S. Cronin, G. Dresselhaus, M. Dresselhaus, J. H. Satcher, Jr.

November 11, 2004

Langmuir

Formation of Carbon Nanostructures in Cobalt- and Nickel-Doped Carbon Aerogels

Ruowen Fu,[1,2] Theodore F. Baumann,[3] Steve Cronin,[1] Gene Dresselhaus,[1] Mildred S. Dresselhaus[1] and Joe H. Satcher, Jr.[3]

[1]Department of Electrical Engineering and Computer Science and Department of Physics, Massachusetts Institute of Technology, Cambridge, Massachusetts 02139

[2]PCFM Laboratory, Zhongshan University, Guangzhou, 510275 China

[3]Lawrence Livermore National Laboratory, Livermore, California 94551

AUTHOR EMAIL ADDRESS: baumann2@llnl.gov

RECEIVED DATE

Abstract. We have prepared carbon aerogels (CAs) doped with cobalt or nickel through sol-gel polymerization of formaldehyde with the potassium salt of 2,4-dihydroxybenzoic acid, followed by ion-exchange with $M(NO_3)_2$ (where M = Co^{2+} or Ni^{2+}), supercritical drying with liquid CO_2 and carbonization at temperatures between 400°C and 1050°C under an N_2 atmosphere. The nanostructures of these metal-doped carbon aerogels were characterized by elemental analysis, nitrogen adsorption, high resolution transmission electron microscopy (HRTEM), X-ray photoelectron spectroscopy (XPS) and X-ray diffraction (XRD). Metallic nickel and cobalt nanoparticles are generated during the carbonization process at about 400°C and 450°C, respectively, forming nanoparticles that are ~4 nm in diameter. The sizes and size dispersion of the metal particles increase with increasing carbonization temperatures for both materials. The carbon frameworks of the Ni- and Co-doped aerogels carbonized below 600°C mainly consist of interconnected carbon particles with a size of 15 to 30 nm. When the samples are pyrolyzed at 1050°C, the growth of graphitic nanoribbons with different curvatures is observed in the Ni and Co-doped carbon aerogel materials. The distance of graphite layers in the nanoribbons is about 0.38 nm. These metal-doped CAs retain the overall open cell structure of metal-free CAs, exhibiting high surface areas and pore diameters in the micro and mesoporic region.

Introduction

Carbon aerogels (CA) are novel mesoporous materials with many interesting properties, such as low mass densities, continuous porosities, high surface areas and high electrical conductivity.[1-4] These properties are derived from the aerogel microstructure, which is a network of interconnected primary particles with characteristic diameters between 3 and 25 nanometers. Because of their unusual chemical and textural characteristics, carbon aerogels are promising materials for use as electrode materials for super capacitors and rechargeable batteries, advanced catalyst supports, adsorbents, chromatographic packing, thermal insulator and a variety of other applications.[5-7] CA's are prepared through the sol-gel polymerization of resorcinol with formaldehyde in aqueous solution to produce organic gels that are supercritically dried and subsequently pyrolyzed in an inert atmosphere.

To expand their potential applications, recent efforts have focused on modification of CA's through the use of doped molecules. One area of significant interest is in the incorporation of metal species into the carbon framework with the goal of modifying the structure, conductivity and catalytic activity of the aerogel.[8-16] We recently reported a new sol-gel technique for the synthesis of metal-doped carbon aerogels that would allow us to control both the amount and the distribution of a desired metal species within the carbon framework.[17-19] This technique, which involves the sol-gel polymerization of resorcinol derivatives containing ion exchange moieties, was shown to be an effective method to uniformly incorporate metal ions into the aerogel matrix. For example, the base-catalyzed polymerization of formaldehyde with the potassium salt of 2,4-dihydroxybenzoic acid produces a K^+-doped hydrogel. The potassium ions in the hydrogel can then be replaced with the desired metal ion through ion exchange and the metal-doped hydrogels can then be processed and carbonized to generate a metal-doped carbon aerogel. We also noted that certain metal ions are reduced during the carbonization process, leading to the formation of nanometer-sized metallic particles that are distributed throughout the carbon matrix.

In this report, we present the synthesis and characterization of cobalt- and nickel-doped carbon aerogels prepared by this ion exchange method. Our interest in the incorporation of these metals into the carbon aerogel framework is due to the fact that these metals are known to catalyze the formation of graphitic structures at relatively low temperatures.[14,20] Since carbon aerogels have low mass densities and high surface areas, the metal-doped derivatives may provide a dilute carbon source for the growth of carbon nanostructures. The formation of graphitic structures within the carbon aerogel framework should modify the electrical and mechanical properties of these materials. This report details the microstructural

characterization of these metal-doped CAs by transmission electron microscopy (TEM), X-ray photoelectron spectroscopy (XPS), X-ray diffraction (XRD) and nitrogen adsorption/desorption analysis.

Experimental Section

Sample Preparation. Metal-loaded dihydroxybenzoate-formaldehyde aerogels (DF-M, where M = Co^{2+} and Ni^{2+}) were synthesized using our previously reported method.[17] In a typical experiment, a suspension of 2,4-dihydroxybenzoic acid (2.9 g, 18.8 mmol) in distilled water (100 mL) was treated with K_2CO_3 (1.29 g, 9.4 mmol) with vigorous stirring. The reaction solution became clear after 0.5 h, when all of the acid was neutralized. Formaldehyde (2.98 g, 37 mmol) was then added to the solution, followed by the catalyst, K_2CO_3 (26 mg, 0.188 mmol). The clear solution was poured into glass molds that were then sealed and the mixture was allowed to cure for 24 h at room temperature and 72 h at 80°C. The resultant K^+-loaded hydrogels were obtained as dark red, transparent monoliths. For preparation of the M^{n+}-loaded organic gels, the K^+-doped hydrogels were soaked in 0.1 M aqueous solution of $M(NO_3)_2$ for 24 h; this procedure was repeated three times. The M^{n+}-loaded hydrogels were washed first with water and then with acetone until the water was completely exchanged and dried with supercritical CO_2 (T_c = 31.1°C, P_c = 7.4 MPa). The above formulation generated DF aerogels with densities between 150 and 200 mg/cm^3. Carbonization of the metal-loaded organic aerogels was performed at temperatures between 400°C and 1050°C for 3 h under an N_2 atmosphere. Following pyrolysis, the densities of the dark brown monoliths were 300 to 350 mg/cm^3. The carbonized materials are denoted as CA-M-T_c, where M = Co or Ni and T_c is the temperature of carbonization.

Characterization. Surface area determination and pore volume and size analysis were performed by Brunauer-Emmett-Teller (BET) and Barrett-Joyner-Halenda (BJH) methods using an ASAP 2000 Surface Area Analyzer (Micromeritics Instrument Corporation).[21] Samples of approximately 0.1 g were heated to 150°C under vacuum (10^{-5} Torr) for at least 24 hours to remove adsorbed species. Nitrogen adsorption data were then taken at five relative pressures from 0.05 to 0.20 at 77K to calculate the surface area by BET theory. Bulk densities of the DF and carbonized aerogels were determined by measuring the dimensions and mass of each monolithic sample. Elemental analyses were performed by Galbraith Laboratories, Knoxville, TN. High-resolution transmission electron microscopy (HRTEM) of the metal-doped aerogels was performed on a JEOL JEM-200CX operating at 200 keV. The images were taken under BF (bright field) conditions and slightly defocused to increase contrast. The XRD pattern was recorded using a

Rigaku 300 X-ray diffractometer with the following measurement conditions: high voltage: 60 kV; current: 300 mA; divergence slit: 1°; scatter slit: 1°; receiving slit: 0.3°; scan mode: continuous; scan type: standard; axis: 2□/□-refl; scan: 5 ° to 85 °; scan speed: 10 °/min; sampling interval, 0.05°. XPS characterization of the aerogels was carried out on an AXIS HIS 165 and ULTRA Spectrometer made by Kratos Analytical Ltd. England, using Al K radiation (energy 1486.6 eV) in a vacuum of 5 x 10^{-9} Torr. Samples were ground into a powder and mounted on a sample holder using double-sided adhesive tape. X-ray slots of 760 by 350 m^2 and an X-ray power of 150 W (15 kV and 10 mA) were used for all the XPS measurements.

Results and Discussion

Synthesis. The objective of this work is to determine the effects that the incorporated metal species has on the carbon aerogel microstructure during the carbonization process. Towards this goal, we prepared Co^{2+}- and Ni^{2+}-doped organic aerogels using our ion exchange process and carbonized these materials at temperatures ranging from 400°C and 1050°C. Following our procedure for the preparation of the copper-doped CA, the synthesis of the metal-doped CA's began with the sol-gel polymerization of the potassium salt of 2,4-dihydroxybenzoic acid (2,4-DHBA) with formaldehyde using potassium carbonate as the base catalyst.[17] As we previously demonstrated, the carboxylate moieties of 2,4-DHBA serve as ion exchange sites for the incorporation of metal species into the gel framework. This process affords K^+-doped DF hydrogels as dark red, transparent monoliths. The cobalt or nickel ions were introduced into the organic gel network through ion exchange. The monolithic wet gels containing potassium ions were soaked in an aqueous solution of the respective $M(NO_3)_2$ salt. To ensure that there was no precipitation or crystallization of residual metal nitrate in the pores of the gel, the monoliths were washed with water following ion exchange. Based on elemental analyses of the dried metal-doped DF aerogels, the ion exchange appears to be nearly complete. Following carbonization, the metal content in the CA's was determined to be 9-10% by elemental analysis. The metal content in these aerogels is two to three times higher than the metal content in CA's prepared by other methods.

Structure and Morphology. We utilized high-resolution transmission electron microscopy (HRTEM) to examine the morphology of the metal-doped CA aerogels. The micrographs of the pre-carbonized M^{2+}-doped organic aerogels show that the aerogel structure consists of a dense network of spherical primary particles with diameters between 15-30 nanometers. These networks define the micro- and mesoporous cavities within the gel network. Most notably, there are no visible metal nanoparticles or precipitated metal salts, indicating that the metal ions are uniformly and molecularly distributed throughout the gels as counter

ions to the carboxylate moieties. Following carbonization, the metal-doped CA's retain the general morphology of the carbon network seen in the pre-carbonized material. The nanopores are still evident, while the carbon network appears to be composed of slightly smaller particles (10 to 15 nm). More importantly, metallic nanoparticles are now evident throughout the carbon framework of the metal-doped CA's. Based on the examination of the metal-doped CA's that were pyrolyzed at different temperatures, we observed that the formation and size of the metal nanoparticles are intimately tied to the carbonization temperature.

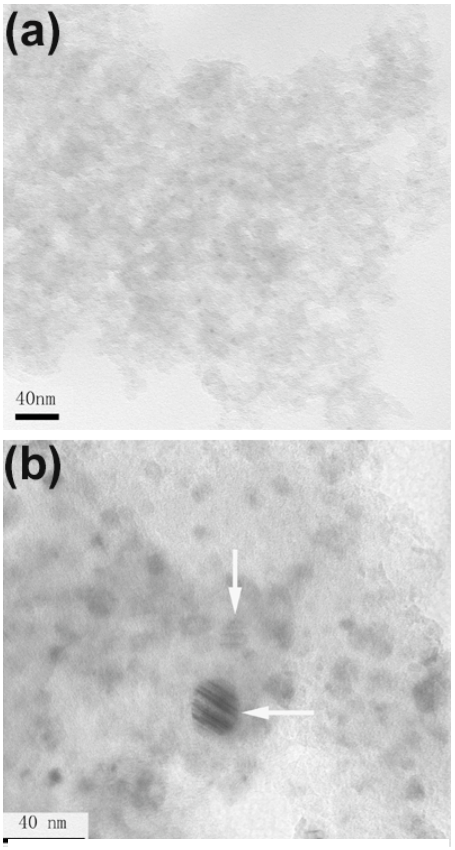

Figure 1. TEM images of CA-Co carbonized at (a) 450°C and (b) 600°C.

For the Co-doped CA's, the TEM micrographs show that small Co particles (~2 nm) begin to form when the material is carbonized at 450°C (Figure 1). The dispersion of these metallic Co particles appears to be quite uniform throughout the carbon matrix. As the carbonization temperature is increased, the average size of the cobalt particles increases as well, with some of the particles as large as 60 nm when the materials are carbonized at 1050°C (Figure 2). It is interesting to note that when the Co-doped aerogels are carbonized as low as 600°C, highly ordered carbon layers start to form around the Co particles (see arrows in Figure 1b), indicating that the cobalt nanoparticles can induce the formation of ordered carbon structures during carbonization. The growth of the graphitic structures in these metal-doped CAs will be discussed later in this section.

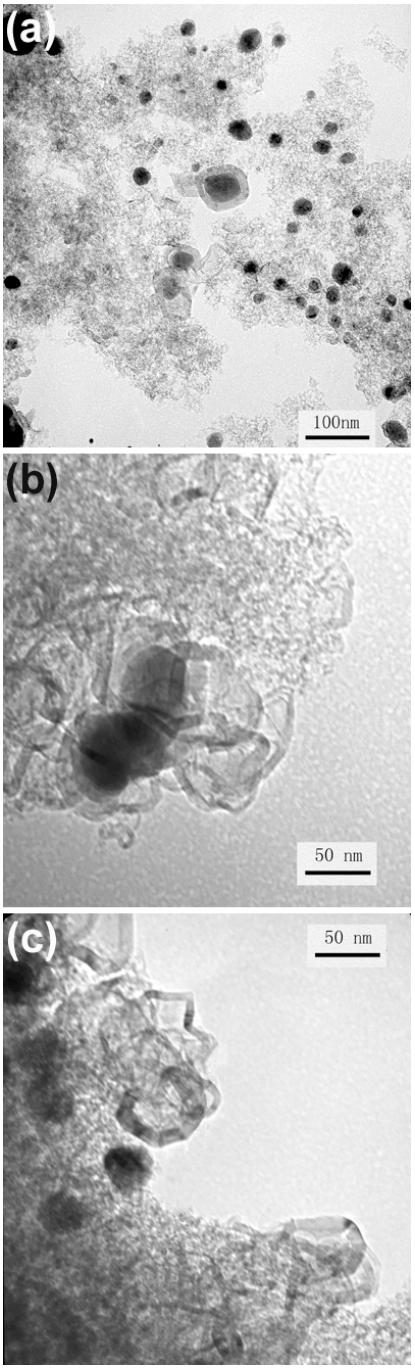

Figure 2. TEM images of CA-Co-1050 showing the Co nanoparticles and graphitic ribbons.

The X-ray photoelectron spectra (XPS) of the Co-doped CAs are almost identical at or below a carbonization temperature of 400°C (Figure 3). When the carbonization temperature increases to 450°C, the $Co_{2p3/2}$ peak of the material moves toward low binding energy and is widened. This peak can be divided into two component peaks with binding energies of 780.5 eV and 778.4 eV, by curve fitting (Figure 4). The component peak at 780.4 eV can be assigned to CoO while the peak at 778.3 eV can be assigned to metallic cobalt, based on reference XPS data.[22] These results indicate that the Co^{2+} ions in the organic aerogel matrix are not directly reduced to metal particles at these low carbonization temperatures. The XRD data for the Co-doped CA's carbonized at different temperatures are consistent with the XPS results (Figure 5). For Co-doped CA's carbonized below 400°C, diffraction peaks corresponding to CoO are apparent in the XRD pattern. When the carbonization temperature exceeded 450°C, peaks for metallic cobalt are observed in the diffraction pattern. The diffraction intensity of the metallic cobalt in the Co-doped CAs grows as the carbonization temperature increases, indicating that the average size of the Co particles is also increasing. When the material is carbonized at 1050°C, diffraction peaks for CoO are no longer visible (Figure 6). Interestingly, the cobalt nanoparticles that form when the aerogels are carbonized at 500°C are active enough that the aerogel ignited spontaneously at room temperature upon removal from the carbonization furnace. This observation is likely due to the small size of the cobalt particles dispersed throughout the carbon matrix. As the size of the Co particles in the aerogel increases, the materials became more stable and the self-ignition was not observed.

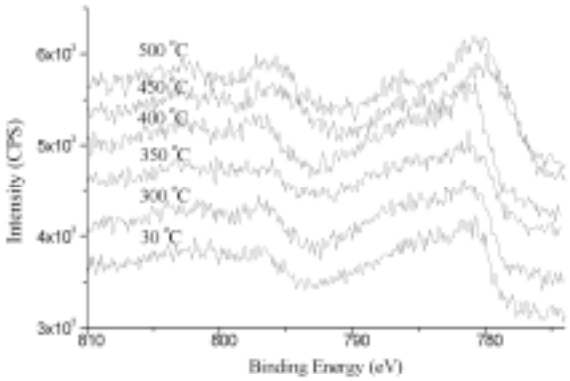

Figure 3. Co2p XPS spectra of CA-Co carbonized at different temperatures.

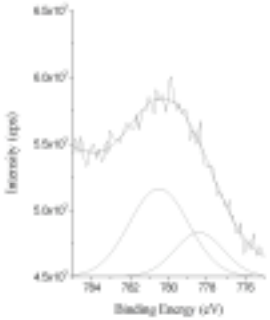

Figure 4. The curve fitting results for the Co $2p_{3/2}$ peak for CA-Co-450.

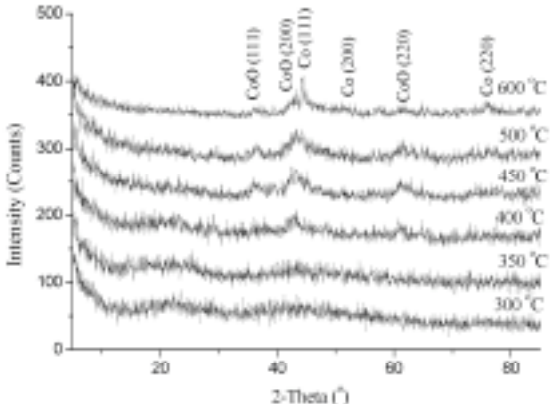

Figure 5. Powder X-ray diffraction patterns for CA-Co carbonized at different temperatures.

For the Ni-doped CAs, transmission electron micrographs show the formation of 2 to 4 nm sized nickel nanoparticles at carbonization temperatures as low as 400°C (Figure 7). As with the Co-doped CAs, the dispersion of the metallic Ni particles appears to be quite uniform throughout the carbon matrix. When the carbonization temperature increases to 600°C, the size of the metallic nickel particles does not change significantly, but the density of the nickel nanoparticles does increase, indicating that more of the nickel ions are reduced into detectable particles. When the Ni-doped material is carbonized at 1050°C, the average size of the Ni particles is greatly increased with many particles in the 200 to 400 nm range (Figure 8). The XPS data shows that there is no reduction of the nickel ion when the aerogels are carbonized below 350°C, based on the positions of Ni_{2p} peaks (Figure 9). As the pyrolysis temperature is increased to 400°C, the $Ni_{2p3/2}$ peak is clearly splits into two component peaks. One peak remains at the original position (~856 eV), while a new peak appears at ~852.7 eV, which can be assigned to the elemental nickel.[22] Unlike the Co-doped materials, there is no evidence that an intermediate oxide of the metal dopant forms during the carbonization process. The XRD results show diffraction pattern for metallic nickel for aerogels carbonized as low as 400°C (Figure 10). The peak intensity of metallic nickel particle increases with increasing carbonization temperature.

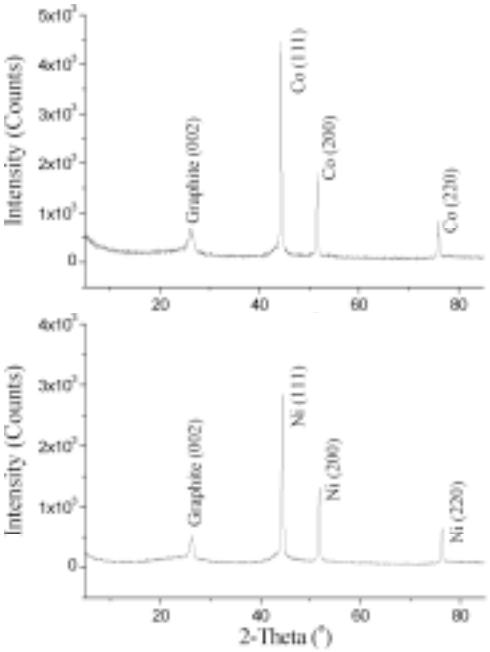

Figure 6. Powder X-ray diffraction patterns for CA-Co-1050 and CA-Ni-1050.

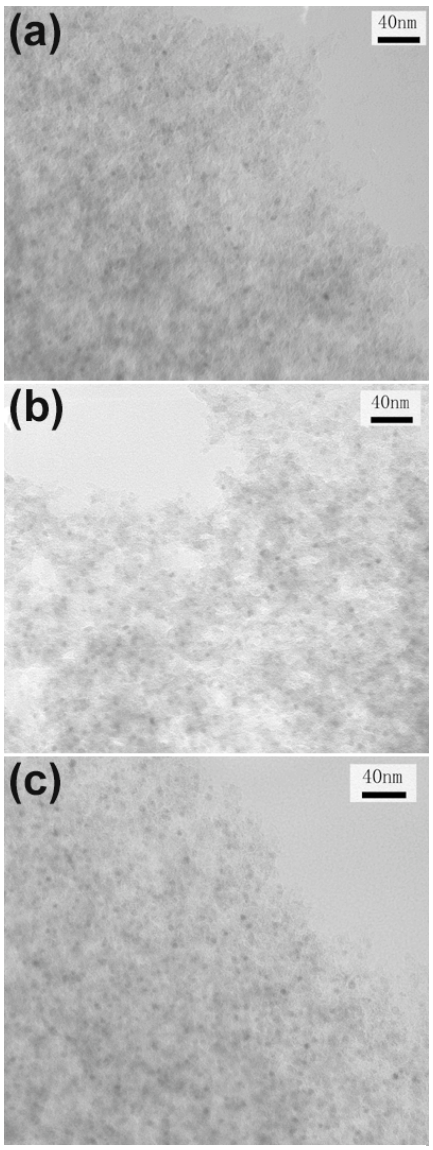

Figure 7. TEM images of CA-Ni carbonized at (a) 400°C, (b) 500°C and (c) 600°C.

The carbon networks of the metal-doped aerogels carbonized at or below 600°C are all very similar, consisting of interconnected spheroidal carbon particles with sizes between 15 and 30 nm. This type of carbon structure is almost the same as those of other carbon aerogels reported in the literature. Therefore,

it is clear that metal-catalyzed formation of graphitic structures does not occur at these lower carbonization temperatures. When the metal-doped aerogels are carbonized at 1050°C, significant changes in the carbon microstructure can be observed. For the Co-doped CA carbonized at 1050°C, the interconnected carbon particles that comprised the aerogel framework are quite different from those found in undoped CAs carbonized at the same temperature. The primary particles in the aerogel skeleton are smaller and many of them no longer have a spheroidal shape. More importantly, graphitic ribbons are now observed throughout the structure, as evidenced by the [002] lattice fringes (Figure 11). The formation of similar structures was observed previously in other metal-doped carbon aerogel systems.[10] In most cases, the graphitic ribbons bend with different curvature, an effect caused by the deformation and twinning of the graphite sheets (Figures 2 and 8).[23,24] In a few areas, we find graphitic ribbons wrapped around the cobalt particles. The width of these graphitic ribbons ranges from several nm to ~20 nm and the distance between graphite layers (D002) was measured to be ~0.38 nm. This interlayer distance is much larger than is typical for graphite, and we attribute that to the fact that these samples were carbonized at relatively low temperatures. Similar graphitic structures are also observed

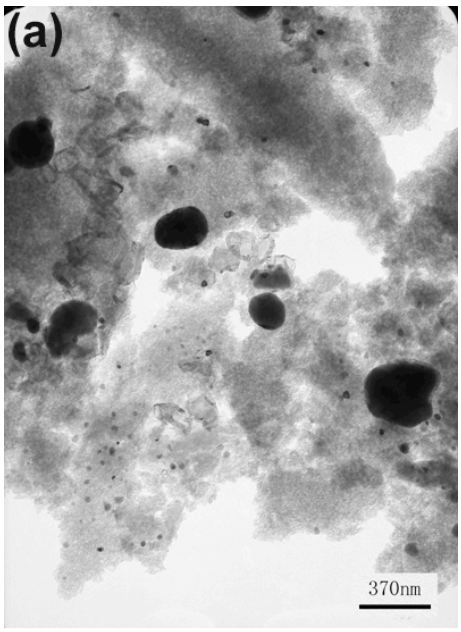

Figure 8. TEM images of CA-Ni-1050 showing the Ni nanoparticles and graphitic ribbons.

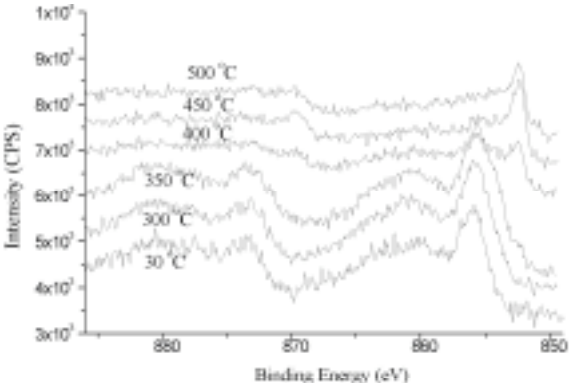

Figure 9. Ni2p XPS spectra of CA-Ni carbonized at different temperatures.

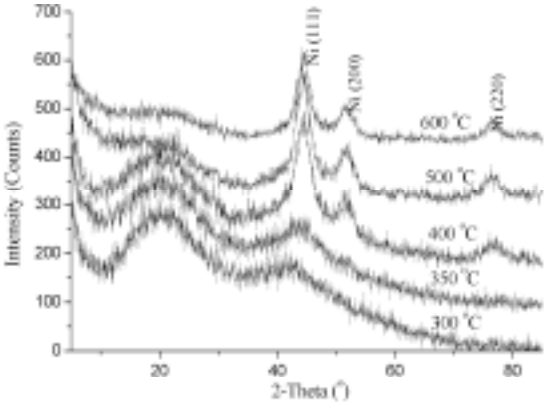

Figure 10. Powder X-ray diffraction patterns for CA-Ni carbonized at different temperatures.

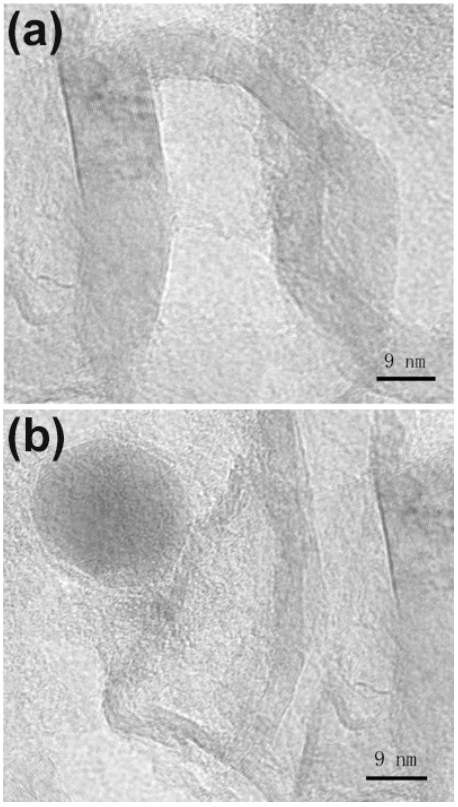

Figure 11. High-resolution TEM images of the graphitic ribbons formed in CA-Co-1050.

in the Ni-doped CAs carbonized at 1050°C. The widths of the graphitic ribbons in the Ni-doped CAs, however, are generally larger than those seen in the Co-doped CAs. In agreement with the TEM results, the XRD data for the Co- and Ni-doped CAs pyrolyzed at 1050°C showed the [002] peak for the graphitic carbon as well as strong diffraction peaks for the metallic particles (Figure 6).

Nitrogen Adsorption/Desorption Analysis. The surface areas, pore volumes and average pore diameters for the metal-doped organic and carbon aerogels were measured using nitrogen adsorption/desorption techniques (Table 1). In general, the metal-doped materials exhibit extremely high surface areas, exceeding 900 m^2/g, and possess pore diameters in the micro and mesoporic (2-20 nm) region. For comparison purposes, we also prepared an undoped carbon aerogel in which the potassium ion was exchanged from the DF matrix with a proton prior to supercritical drying and pyrolysis, denoted as CA-H-1050. This material possesses textural properties comparable to those of the M-doped carbon aerogels, indicating that, despite the presence of the dopant, these new carbon materials retain the overall pore structure of the metal-free carbon aerogels. Each of the samples exhibited an adsorption isotherm of type IV and showed a hysteresis loop (H1) at high relative pressures, a feature that is typically associated with capillary condensation within mesopores.[25] These results are in agreement with the transmission electron micrographs for these materials that showed interconnected networks of spherical primary particles defining meso- and microporous channels.

Conclusion

Incorporation of metal dopants into CA's is a powerful way to control both the structure and physical properties of these materials. In this report, we describe the synthesis and characterization of a new series of metal-doped CAs, where M = Ni and Co. For the synthesis, we employed our approach that utilizes the sol-gel polymerization of resorcinol derivatives containing ion exchange moieties, which ensures a uniform distribution of metal species throughout the aerogel structure. One of the exciting features of these novel materials is that carbonization of the metal-doped organic aerogels results in the formation of metal

nanoparticles as well as growth of carbon nanostructures within the carbon aerogel framework. These changes should have a significant impact on the physical properties of the CAs and, as such, we are currently investigating the transport and mechanical properties of the metal-doped materials. These studies will be the subject of a future report and should provide additional insight into the structure-property relationship associated with these new materials.

Acknowledgements. Work was performed under the auspices of the U.S. Department of Energy by UC, Lawrence Livermore National Laboratory under contract number W-7405-ENG-48. This research was supported by LLNL subcontract B518047 and partially supported by the Team Project of Guangdong Science Foundation and the Foundation for the Key Teachers in China.

Table 1. Physical properties of the doped carbon aerogels carbonized at 1050°C.

Aerogel	Dopant (%M)	Specific Surface Area (m^2/g)	Average Pore diameter (nm)	Pore volume (cm^3/g)
CA-Co-1050	9.9	954	21.0	3.7
CA-Ni-1050	9.2	1103	20.8	4.3
CA-H-1050	0	907	23.5	3.7

References

1 Pekala, R. W. *J. Mater. Sci.* **1989**, *24*, 3221.

2 Pekala, R. W.; Alviso, C. T.; Kong, F. M.; Hulsey, S. S. *J. Non-Cryst. Solids* **1992**, *145*, 90.

3 Pekala, R. W.; Alviso, C. T.; LeMay, J. D. In *Chemical Processing of Advanced Materials*; Hench, L. L., West, J. K., Eds.; J. Wiley & Sons: New York, **1992**; p. 671.

4 Kong, F. M.; LeMay, J. D.; Hulsey, S. S.; Alviso, C. T.; Pekala, R. W. *J. Mater. Sci.* **1993**, *8*, 3100.

5 Saliger, R.; Fischer, U.; Herta, C.; Fricke, J. *J. Non-Cryst Solids*, **1998**, *225*, 81.

6 Yang, K.L.; Ying, T.Y.; Yiacoumi, S.; Tsouris, C.; Vittoratos, E. S. *Langmuir* **2001**, *17*. 1961.

7 Pekala, R.W.; Farmer, J.C.; Alviso, C.T.; Tran, T.D.; Mayer, S.T.; Miller, J.M.; Dunn, B. *J. Non-Cryst Solids*, **1998**, *225*, 74.

8 Bekyarova, E.; Kaneko, K. *Adv. Mater.* **2000**, *12*, 1625.

9 Bekyarova, E.; Kaneko, K. *Langmuir* **1999**, *15*, 7119.

10 Maldonado-Hódar, F. J.; Moreno-Castilla, C.; Rivera-Utrilla, J.; Hanzawa, Y.; Yamada, Y. *Langmuir* **2000**, *16*, 4367.

11 Maldonado-Hódar, F. J.; Ferro-García, M. A.; Rivera-Utrilla, J.; Moreno-Castilla, C. *Carbon*, **1999**, *37*, 1199.

12 Moreno-Castilla, C.; Maldonado-Hódar, F. J.; Rivera-Utrilla, J.; Rodríguez-Castellón, E. *Appl. Catal. A* **1999**, *183*, 345.

13 Moreno-Castilla, C.; Maldonado-Hódar, F. J. *Phys. Chem. Chem. Phys.* **2000**, *2*, 4818.

14 Moreno-Castilla, C.; Maldonado-Hódar, F. J.; Carrasco-Marin, F.; Rodriguez-Castellon, E. *Langmuir* **2002**, *18*, 2295.

15 Miller, J. M.; Dunn, B. *Langmuir* **1999**, *15*, 799.

16 Fu, R.; Dresselhaus, M. S.; Dresselhaus, G.; Zheng, B.; Liu, J.; Satcher, J. H.; Baumann, T. F. *J. Non-Cryst. Solids* **2003**, *318*, 223.

17 Baumann, T. F.; Fox, G. A.; Satcher, J. H.; Yoshizawa, N.; Fu, R.; Dresselhaus, M. S. *Langmuir* **2002**, *18*, 7073.

18 Fu, R.; Yoshizawa, N.; Dresselhaus, M. S.; Dresselhaus, G.; Satcher, J. H.; Baumann, T. F. *Langmuir* **2002**, *18*, 10100.

19 Fu, R.; Lin, Y. M.; Rabin, O.; Dresselhaus, G.; Dresselhaus, M. S.; Satcher, J. H.; Baumann, T. F. *J. Non-Cryst. Solids* **2003**, *317*, 247.

20 Bethune, D. S. ; Kiang, C. H.; DeVries, M. S.; Gorman, G.; Savoy, R.; Vazquez, J.; Beyers, R. *Nature* **1993**, *363*, 605.

21 Gregg, S. J.; Sing, K. S. W. *Adsorption, Surface Area and Porosity*, 2nd ed.; Academic Press: London, **1982**.

22 Moulder, J. F.; Stickle, W. F.; Sobol P. E.; Bomben, K. D. *Handbook of X-ray Photoelectron Spectroscopy*, J. Chastain, ed.; Perkin-Elmer: Minnesota, **1979**.

23 Dresselhaus, M. S.; Dresselhaus, G.; Eklund, P. C. *Science of Fullerences and Carbon Nanotubes*, Academic Press, **1995**.

24 Oleg P. Krivoruchko, Nadezhda I. Maksimova, Vladimir I. Zaikovskii, Aleksei N. Salanov, *Carbon*, **2000**, *38*, 1075.

25 Rouquerol, F.; Rouquerol, J.; Sing, K. *Adsorption by Powders and Porous Solids: Principles, Methodology and Applications*, Academic Press: London, **1999**.

Table of Contents Graphic: